Quantification of Hyporheic Nitrate Removal at the Reach Scale: Exposure Times vs. Residence Times

Sven Frei, Stefan Durejka, Hugo Le Lay, Zahra Thomas, Benjamin S. Gilfedder

Frei S. (Orcid ID: 0000-0002-1818-8246)

Thomas Z. (Orcid ID: 0000-0001-5090-0988)

Gilfedder B.S. (Orcid ID: 0000-0002-6169-5198)

Title: Quantification of Hyporheic Nitrate Removal at the Reach Scale: Exposure Times vs. Residence Times

S. Frei[1], S. Durejka[1,2], H. Le Lay[3,4] , Z.Thomas[3,4], B.S. Gilfedder[1,2]

[1]Department of Hydrology, Bayreuth Center of Ecology and Environmental Research (BAYCEER), University of Bayreuth, Germany
[2]Limnological Research Station, Bayreuth Center of Ecology and Environmental Research (BAYCEER), University of Bayreuth, Germany
[3]UMR SAS, INRA, AGROCAMPUS OUEST, 35042 Rennes, France
[4]LTSER "Zone Atelier Armorique", Rennes, France

Corresponding author: S. Frei (sven.frei@uni-bayreuth.de)

Key Points:

- Lumped parameter modeling of hyporheic nitrate removal by applying the exposure time concept.
- Exposure time distributions are derived from analytical residence time distributions and reaction kinetics for hyporheic oxygen consumption.
- Using exposure times rather than residence times is likely to lead to more realistic estimates for nutrient removal in the hyporheic zone

This article has been accepted for publication and undergone full peer review but has not been through the copyediting, typesetting, pagination and proofreading process which may lead to differences between this version and the Version of Record. Please cite this article as doi: 10.1029/2019WR025540

Abstract

The rate of biogeochemical processing associated with natural degradation and transformation processes in the hyporheic zone (HZ) is one of the largest uncertainties in predicting nutrient fluxes. We present a lumped parameter (LPM) model that can be used to quantify the mass loss for nitrate in the HZ operating at the scale of river reaches to entire catchments. The model is based on using exposure times (ET) to account for the effective timescales of reactive transport in the HZ. Reach scale ET distributions are derived by removing the portion of hyporheic residence times (RT) associated with flow through the oxic zone. The model was used to quantify nitrate removal for two scenarios: 1) a 100 m generic river reach and 2) a small agricultural catchment in Brittany (France). For the field site hyporheic RT are derived from measured in-stream ^{222}Rn activities and mass balance modelling. Simulations were carried out using different types of RT distributions (exponential, power-law and gamma-type) for which ET were derived. Mass loss of nitrate in the HZ for the field site ranged from 0-0.45 kg d^{-1} depending on the RT distribution and the availability of oxygen in the streambed sediments. Simulations with power law ET distribution models only show very little removal of nitrate due to the heavy weighting towards shorter flow paths that are confined to the oxic sediments. Based on the simulation results, we suggest that ET likely lead to more realistic estimates for nutrient removal.

1. Introduction

The hyporheic zone (HZ) is an important interface between surface water and groundwater that hosts an array of biogeochemical processes contributing to nitrogen cycling and removal in river networks. Nitrate processing in the HZ results from different biogeochemical reaction pathways that are central to the self-purification capacities of rivers and streams [*Burgin and Hamilton*, 2007]. Heterotrophic processes such as respiratory denitrification or fermentative dissimilatory nitrate reduction to ammonium (DNRA) besides nitrate require a suitable or-

ganic carbon source. While denitrification is a permanent sink for nitrate in the HZ, fermentative DNRA is considered as an intermediate sink as it transforms nitrate into ammonium. Produced ammonium in the HZ can be converted back to nitrate by nitrification under appropriate biogeochemical conditions (i.e. presence of oxygen). Pathways for nitrate removal that do not rely on the availability of an organic carbon source (chemoautotrophic processes) include iron and sulfur driven nitrate reduction as well as anaerobic ammonium oxidation (ANAMOX).

Although, the relative contribution of the these processes to nitrate removal at the catchment scale is still unclear [*Burgin and Hamilton*, 2007], all heterotrophic and chemoautotrophic nitrate removal pathways are controlled by the complex interplay of 1) microbiology, 2) substrate availability, 3) the presence and absence of oxygen as well as 4) the hydrodynamic flow conditions in the stream [*Marzadri et al.*, 2012; *Zarnetske et al.*, 2011; *Briggs et al.*, 2014]. Oxygen availability can change within centimeters for rippled bedforms [*Kessler et al.*, 2013] to meters in gravel bars, river banks and meander bends [*Trauth et al.*, 2013; *Gu et al.*, 2012]. Stream morphological features such as riffle/pool sequences or rippled bedforms are controlling factors for the interaction between hydrology and biogeochemistry and are of particular importance for nitrate processing in river systems [*Frei et al.*, 2018]. Site specific features such as regional groundwater flow [*Trauth et al.*, 2013] or streambed morphology affect hyporheic water exchange fluxes and residence times (RT) in the HZ [*Cardenas et al.*, 2004; *Boano et al.*, 2014]. RT have been identified as key a parameter in hyporheic nutrient removal [*Briggs et al.*, 2014; *Zarnetske et al.*, 2011].

A detailed process understanding of how hydrological and biogeochemical processes mechanistically interact in the HZ is one part of an improved and quantitative understanding of riverine nutrient cycling. The latter is especially important when assessing the impact of climate

change with its potential to fundamentally change local to regional hydrological cycles, biogeochemical kinetics as well as interactions and feedbacks among these factors [*Lohse et al.*, 2009]. However, quantification of hyporheic nutrient fluxes and turnover on spatial scales beyond individual bedforms and upscaling results from local studies to catchment scales is rarely addressed in the literature. Exceptions are the work of *Gomez-Velez et al.* [2015] and *Kiel and Cardenas* [2014] who estimated denitrification capacities of the HZ for the entire Mississippi catchment and *Pittroff et al.* [2017] who quantified nitrate removal rates for a 32 km reach of the Roter Main River in South Germany.

Lumped parameter models (LPM) are modeling frameworks well suited for upscaling local nutrient cycling in the HZ to whole catchments [*Pittroff et al.*, 2017]. Instead of simulating the governing physical and biogeochemical processes explicitly, LPMs usually use some kind of probability-density function (*pdf*) to account for transport and degradation of solutes in hydrological systems. The commonly used practice of dating groundwater using radioactive conservative tracers such as Tritium is based on applying a LPM with an associated *pdf* to simulate a catchment's response to a known input function [*Cartwright et al.*, 2018; *Małoszewski and Zuber*, 1982; *Morgenstern et al.*, 2010]. For conservative tracers, the *pdf* is identical to the RT distribution (pdf_{RT}), defining the timescales of water transport in the subsurface. For radioactive tracers decay occurs uniformly along subsurface flow paths and RT are equal to the effective reaction times in the catchment [*Frei and Peiffer*, 2016]. However, biogeochemical processes that occur in hyporheic systems such as denitrification, sulphate reduction, and methane production are redox-sensitive and microbiologically mediated reactions that only take place under appropriate biogeochemical conditions (e.g. in the presence of bioavailable organic carbon or absence of oxygen) [*Burgin and Hamilton*, 2007]. Conditions that favor anaerobic processes are not uniformly distributed in non-well mixed systems such as catchments, wetlands, lake sediments or the HZ. Consequently, for redox-sensitive

solutes RT are usually not equal to the timescales where biogeochemical reactions actually occur. In this case the pdf_{RT} is not an appropriate *pdf* for quantifying nutrient removal in LPMs [*Frei and Peiffer*, 2016]. One exception is oxygen which reacts immediately with organic carbon on entering the subsurface during microbial respiration.

As the HZ is a non-well mixed system exposure times (ET) instead of RT are a better estimator of the effective timescales for reactive transport. However, for the HZ, the RT is often presented as a key parameter used in quantifying hyporheic nutrient removal [*Cardenas et al.*, 2004; *Boano et al.*, 2014; *Pittroff et al.*, 2017; *Runkel*, 1998]. The concept of ET originally was introduced to account for non-uniform biogeochemical conditions in non-well mixed hydrological system such as aquifers or catchments and to characterize effective timescales available for reaction [*Ginn*, 1999; *Seeboonruang and Ginn*, 2006]. By definition, ET represent the timescales over which a material has the opportunity to react [*Oldham et al.*, 2013]. The concept of ET has been used to simulate bio-reactive transport in porous media [*Sanz-Prat et al.*, 2016] and to describe the hydrological controls on redox-sensitive reactions in wetland ecosystems [*Frei and Peiffer*, 2016].

In this work we present a LPM that can be used to quantify hyporheic nitrate removal rates in streams and rivers at reach to catchment scales by incorporating ET. We introduce a simple method to derive ET distributions (pdf_{ET}) based on a priori defined hyporheic pdf_{RT} and oxygen consumption kinetics in the HZ. The novelty of the approach is that pdf_{ET} are directly derived from analytical pdf_{RT} by introducing a so-called threshold factor that accounts for the presence of oxygen in the HZ. The LPM is first applied to a simple hypothetical scenario representing a generic river reach to study how hyporheic nitrate removal depends 1) on the shape of the hyporheic pdf_{RT} and 2) the kinetics of oxygen consumption in the streambed sediments. As a more realistic scenario the LPM is later applied to quantify hyporheic nitrate

removal for a 2.3 km long stream in a sub-catchment of the International Long Term Ecosystem Research Catchment (LTSER), Brittany, France. For the field application we derive the relevant parameters for the LPM from a Radon-222 (^{222}Rn) mass balance simulation previously described in *Frei and Gilfedder* [2015] and *Pittroff et al.* [2017].

2. Theory

2.1 Representing Hyporheic Nitrate Removal

As part of the LPM we assume that nitrate is permanently removed from the system by anaerobic reaction pathways. We do not account for reactions that form inorganic nitrogen species via decomposition of organic nitrogen (e.g. ammonium) or incomplete nitrate removal pathways that lead back to nitrate via oxidation. This implies that the LPM treats the HZ solely as a permanent sink for nitrogen and excludes production of nitrate in the stream sediments through nitrification. Further we do not explicitly distinguish between the various nitrate reaction pathways outlined in the introduction. Rather we assume that processes responsible for nitrate removal can be lumped into one effective kinetic model that can be applied at the reach scale and thus define nitrate removal as the mass loss of nitrate from the stream via a single bulk reaction kinetic in the HZ. The presented LPM is based on the rules of linear time-invariant (LTI) system theory [*Hespanha*, 2018]. For LTI systems the in- and output variables can be mapped by applying the superposition theorem using a time-invariant impulse-response function. This LPM differs from previous models like OTIS [*Runkel*, 1998] by explicitly differentiating between timescales of water transport (RT) and effective timescales of reaction (ET) in the HZ. The LPM also includes the possibility to work with non-exponential models for representing RT and ET in the HZ, such as gamma or power law distributions. In the following we will describe how hyporheic nitrate removal is represented as part of a convolution framework that is implemented into the LPM.

Nitrate removal in the HZ can be simulated for a single stream reach by 1) assuming that permanent nitrate removal occurs as soon as water infiltrates into the hyporheic sediments as commonly done in the past (i.e. RT = ET), or 2) that nitrate removal processes are initially suppressed by the presence of oxygen in shallow layers of the streambed sediments (i.e. RT ≠ ET). In the first case the pdf_{RT} [T^{-1}] can be used to describe the effective timescales of reaction, where for the second case the timescales of reaction are described by a pdf_{ET} [T^{-1}]. By using either pdf_{RT} or pdf_{ET} as impulse-response functions, the nitrate output concentration C_{out} [ML^{-3}] for water leaving the HZ can be estimated by convolution and nitrate removal for a single stream reach R_{NO3} [$M\ T^{-1}$] (in the latter referred to as hyporheic nitrate removal) of length Δx [L] can be quantified:

$$R_{NO3} = q_H \Delta x (C_{in} - C_{out})$$
$$C_{out}(\tau) = \int_0^{\infty} C_{in}(\tau - z) e^{-k_{NO3} z} \cdot pdf_{RT/ET}(z) dz \quad (1)$$
$$q_H = \frac{wh\Theta}{\tau_m}$$

In Equation 1, C_{out} [ML^{-3}] and C_{in} [ML^{-3}] represent the nitrate concentrations leaving and entering the HZ respectively, z [T] represents a dummy variable necessary for carrying out the integration and k_{NO3} [T^{-1}] is an effective first order reaction constant for hyporheic nitrate removal processes and q_H [L^2T^{-1}] is the steady state hyporheic water flux where the water fluxes entering and leaving the HZ are equal (net flux = 0). In this study we assume that C_{in} for a single stream reach is constant. For steady state conditions, the reach-averaged hyporheic flux q_H can be estimated based on the stream width w [L], the hyporheic exchange depth h [L] the mean RT of water in the HZ τ_m [T] and the porosity of the streambed sediments Θ [-] [*Cook*, 2013; *Runkel*, 1998]. By assuming that C_{in} is constant over a reach and applying an

exponential pdf_{RT}, Equation 1 can be solved analytically yielding $C_{out} = C_{in} \cdot \frac{1}{\tau_m k_{NO3} + 1}$. For non-exponential pdf_{RT} such as power law or gamma-type models, the convolution integral in Equation 1 can be solved numerically using adaptive quadrature techniques. When the presence of oxygen suppresses hyporheic nitrate removal processes, the convolution integral in Equation 1 is carried out by using a pdf_{ET} instead of a pdf_{RT}.

2.2 Deriving Exposure Time Distributions

The pdf_{ET} required to carry out the convolution in Equation 1 is derived from a corresponding reach scale pdf_{RT} that is assumed to be known a priori. For a given pdf_{RT} the basic concept of deriving pdf_{ET} is illustrated in Figure 1.

For a typical hyporheic flow cell (Figure 1B) the timescales of hyporheic water flow are defined by pdf_{RT} (Figure 1A). However for the situation where RT ≠ ET some of the flow paths through aerobic areas do not contribute to hyporheic nitrate removal. This time lag between water infiltrating into the HZ and the initiation of hyporheic nitrate removal processes can be described by introducing an isochrone a [T] (Figure 1B). Here a represents the characteristic time for which the majority of oxygen is already consumed and in the latter is referred to as threshold factor. Along flow paths where $\tau < a$ hyporheic nitrate removal processes are assumed to be inactive due to the presence of oxygen. Based on the specific value of a, which can be estimated from known reaction kinetics for oxygen consumption (e.g. via respiration as presented in 2.3) the pdf_{ET} can be derived as follows:

$$pdf_{ET}(\tau') = A_r^{-1} pdf_{RT}(\tau + a)$$
$$A_r = \int_a^{\infty} pdf_{RT}(\tau) d\tau = \int_0^{\infty} pdf_{RT}(\tau + a) d\tau \quad (2)$$

In Equation 2 and as indicated in Figure 1A the expression $\tau+a$ [T] shifts the pdf_{RT} to the left by a constant time a. This shift ensures that the time classes $\tau < a$ in the pdf_{RT} do not contrib-

ute to hyporheic nitrate removal if the convolution in Equation 1 is carried out from $\tau = 0$ to ∞. A_r [-] in Equation 2 represents a scaling factor that ensures that $\int_0^{\infty} pdf_{ET}(\tau')d\tau' = 1$ which is necessary to carry out the convolution integral as part of Equation 1. Finally, to estimate the hyporehic nitrate removal within the anaerobic areas of the HZ the effective hyporheic water flux q_{ET} [L^2T^{-1}] needs to be calculated using Equation 3. For the situation where $a = 0$ and RT = ET, q_{ET} is equal to q_H.

$$R_{NO3} = q_{ET}\Delta x(C_{in} - C_{out})$$
$$q_{ET} = q_H \int_a^{\infty} pdf_{RT}(\tau)d\tau = q_H A_r \quad (3)$$

2.3 Derivation of the threshold factor from reaction kinetics

The threshold factor a is the central parameter necessary to define a pdf_{ET} based on a priori known pdf_{RT}. The threshold factor can either be derived directly from field observations or alternatively from known reaction kinetics for oxygen consumption in the HZ. In both cases a represents a specific period of time needed for dissolved oxygen concentrations to drop below a critical value O_{2crit} [ML^{-3}] after which anaerobic hyporheic nitrate removal pathways are initiated. O_{2crit} as part of this study is defined as the concentration where only 5% of the initial oxygen O_{2init} [ML^{-3}] is still available. Based on this 5% criterion, the time a needed to reach O_{2crit} assuming a 0^{th}-order, 1^{st}-order or Monod reaction kinetics for oxygen consumption processes can be estimated according to Equations 4-6. Here K_{O2} [$ML^{-3}T^{-1}$] and k_{O2} [T^{-1}] represent 0^{th}- and 1^{st} -order reaction constants respectively and v_{O2max} [$ML^{-3}T^{-1}$] is the substrate utilization rate and Ks_{O2} [ML^{-3}] is the substrate concentration at half v_{O2max} for Monod kinetics. Alternatively, measured oxygen profiles in combination with a RT tracer can also be used to derive a suitable threshold value. For example *Pittroff et al.* [2017] measured oxygen availability at various depths of the HZ and concurrently used ^{222}Rn to estimate vertical pro-

files for hyporheic water RT. This resulted in an oxygen vs. RT relationship that could be used to derive the threshold factor *a* for a specific field site.

$$a = 0.95\frac{O_{2init}}{K_{O2}} \quad (4)$$

$$a = -\frac{1}{k_{O2}}\ln(0.05) \quad (5)$$

$$a = \frac{-0.95O_{2init} + Ks_{O2}\ln(0.05)}{-v_{O2max}} \quad (6)$$

3. Applications

The LPM was applied to two different cases. The first application represents a simple test case scenario of a single generic river reach. The generic river reach scenario was used to investigate how the combination of different types of analytical pdf_{RT} models in combination with a large range of possible threshold factors *a* affect reach-scale hyporheic nitrate removal. Additionally the LPM was applied to a small stream (*Villqué*) located in Northern France. The model was used to quantify hyporheic nitrate removal for 13 different stream reaches over a total distance of 2.4 km, with each reach characterized by a separate pdf_{RT} and pdf_{ET}. For the field case hyporheic characteristics for the individual reaches such as τ_m and hyprheic depth *h* were estimated using stream ^{222}Rn measurements and mass balance modeling with the model FINIFLUX [*Frei and Gilfedder*, 2015]. At this point we explicitly want to mention that the LPM framework does not necessarily require a ^{222}Rn mass balance with the only pre-requisite being some way to estimate a mean hyporheic RT and hyporheic exchange depth *h* for a given pdf_{RT}.

3.1 Generic River Reach

τ_m and the threshold factor *a* both are primary control variables governing the water flux through the HZ and hyporheic nitrate removal. The range of published values for τ_m for the HZ varies considerably in literature. Moreover, there are a number of different reaction kinet-

ics used to represent aerobic respiration in the HZ from which the threshold factor *a* can be derived. Values for τ_m, in *Trauth et al.* [2014] range between 1.44 and 6.30 hours for a gravel bar depending on the turbulent in-stream flow conditions and the flux of upwelling groundwater which can suppress hyporheic exchange. *Haggerty et al.* [2002] provides a range of 0.1 to 30 hours for τ_m based on a compilation of existing tracer studies. *Gomez-Velez et al.* [2015] give a characteristic timescale for oxygen consumption (threshold factor *a*) of ~ 1 hour while *Vieweg et al.* [2016] use a threshold factor of ~24 hours based on modeling and field observations. *Kiel and Cardenas* [2014] give a value estimated from field and laboratory studies for the Mississippi basin of a = 6.9 h. A sensitivity analysis was performed for the generic river reach scenario to account for the wide range of reported values for τ_m and *a*, and to test the influence of different combinations of these parameters on hyporheic nitrate removal. The generic reach represents a hypothetical river reach for which τ_m and *a* are systematically varied between 0 and 30 hours. The parameterization of the generic river reach is shown in Table 1. Besides the parameters introduced previously *Qs* [L^3T^{-1}] in Table 1 represents the stream discharge.

For the generic river reach scenario, three different types of analytical RT distributions models were used to represent pdf_{RT}: 1) an exponential model (Eq. 7), 2) a power law distribution with exponential cutoff (Eq. 8) and 3) a gamma-type distribution (Eq. 9).

$$pdf_{RT,\exp}(\tau) = \frac{1}{\tau_m} \cdot e^{\frac{\tau}{\tau_m}} \quad (7)$$

$$pdf_{RT,power}(\tau) = \frac{\beta_P^{\,1-\alpha_p}}{\Gamma(1-\alpha_P, \beta_P \tau_{\min})} \tau^{-\alpha_p} e^{-\beta_p \tau}$$
$$\tau_m = \int_{\tau_{\min}}^{\infty} \tau \cdot pdf_{RT,power}(\tau) d\tau \quad (8)$$

$$pdf_{RT,gamma}(\tau) = \frac{\tau^{\alpha_G - 1}}{\beta_G{}^{\alpha} \Gamma(\alpha)} e^{-\frac{\tau}{\beta_G}} \quad (9)$$

$$\tau_m = \int_0^{\infty} \tau \cdot pdf_{RT,gamma}(\tau) d\tau = \beta_G \alpha_G$$

The parameters α_G [-], α_P [-], β_G [T] and β_P [T^{-1}], in Equation 8 and 9 represent shape and scaling parameters while τ_{min} [T] in Equation 8 is a minimum time class necessary to define the power law distribution model. All pdf_{RT} models are normalized in such a way such that $\int_{\tau=0;\tau_{min}}^{\infty} pdf_{RT}(\tau) d\tau = 1$. For the power law and gamma-type distribution models it is possible to represent a variety of differently shaped pdf_{RT} by adjusting the corresponding shape factors α_G and α_P (Figure 2). For the power law model τ_{min} was uniformly set to 0.001 hours throughout this study. For α_G = 1 the gamma-type model is identical to an exponential distribution (Figure 2A). For all distributions shown in Figure 2 the parameters β_G and β_P were set to achieve a common mean value for hyporheic RT of τ_m = 1.5 hours. For the sensitivity analysis we used a set of pre-defined shape parameters (α_G, α_P) while the parameters for β_G and β_P were set to a value that correspond to τ_m in the range of 0 and 30 hours. For the generic river reach we compare the simulation outputs in term of hyporheic nitrate removal efficiencies E [-] defined as the hyporheic nitrate removal divided by the in-stream nitrate mass flux (Equation 10):

$$E = \frac{R_{NO3}}{Cin \cdot Q_s} \quad (10)$$

3.2 Field case: Vilqué catchment

The field case represents a small stream at the Zone Atelier Armorique (ZAAr), which is a part of the Long-Term Socio-ecological Research platform (LTSER) [*Mirtl et al.*, 2018; *Haase et al.*, 2018; *Thomas et al.*, 2019] located in the northwest of France near the town of Pleine–Fougères (Figure 3). In Brittany (north west of France) stream biodiversity and water quality have been strongly affected by the intensification of agriculture. Surface water ecosystems (lakes, rivers, and estuaries) have been highly degraded, especially due to nitrate

excess [*Thomas et al.*, 2016]. Average nitrate concentrations increased from 9 mg l^{-1} in 1976 to 65 mg l^{-1} in 1989 and have stabilized at about 70 mg l^{-1} as of 2008 [*Cann*, 1998], exceeding numerous regulatory limits (European Nitrate directive 1991). The ecological consequence of the nitrate loading to the coastal zone has been multiple algal blooms along the Brittany coastline. The 2.3 km stream, known locally as *Vilqué*, drains a 2.3 km² sub catchment of the LSTER (Figure 3). The catchment consists of predominantly agricultural land including dairy and low intensity crops. Bedrock geology is mainly composed of metamorphic altered sedimentary rocks, schists and hornfels from the Proterozoic (Brioverian). Intrusive granodiorites of Cadomian age are found in the southernmost part of the catchment and upstream of our first sampling point (seismic cross section in the supplement).

^{222}Rn sampling was performed in spring 2017. The discharge prior to and during sampling was constant ranging between 0.002 m^3 s^{-1} at the most upstream location to 0.031 m^3 s^{-1} at the catchment outlet. Discharge was measured by using salt pulse tracer measurements (sudden-injection method [*Rantz*, 1982]) for the upstream reaches and an induction flow meter using the two-point method [*Rantz*, 1982] for the stream reaches located downstream. Fourteen 1 liter stream samples for ^{222}Rn and nitrate analysis were collected from the headwater area of the *Vilqué* stream to its confluence with *l'Hermitage* at intervals of 100 m and 500 m (Figure 3). ^{222}Rn was measured in the field using a RAD7 Radon in air detector by applying a method similar to *Lee and Kim* [2006] which we have also used in previous work [*Cartwright et al.*, 2018; *Pittroff et al.*, 2017; *Cartwright and Gilfedder*, 2015]. Each sample was purged for 5 minutes and then counted for 1 hour. Replicate samples were run with a precision of better than ±15% relative standard deviation (RSD). Samples for nitrate analysis were first filtered through 0.45 µm filters and then stored at 4°C until measured by ion chromatography (Metrohm GmbH). Precision was better than ±5% RSD.

3.2.1 Field case: ^{222}Rn Mass Balance Modelling

Steady state mass balance modelling for in-stream ^{222}Rn was performed using the model FINIFLUX described in detail in *Frei and Gilfedder* [2015]. FINIFLUX numerically solves the mass balance equation for in-stream ^{222}Rn [M L^{-3}] on the reach scale (Equation 11) by using a Petrov-Galerkin Finite Element scheme based on in-stream ^{222}Rn measurements.

$$Q_s \frac{d^{222}Rn}{dx} = I(^{222}Rn_{gw} - ^{222}Rn) - k_{\deg} w\, ^{222}Rn - dw\lambda_{Rn}\, ^{222}Rn + \alpha_1 - \alpha_2\, ^{222}Rn + \frac{Q_r}{R_L}\left(^{222}Rn_{trib} - ^{222}Rn\right) \quad (11)$$

Here, x [L] is the 1D stream length, w [L] is the mean stream width, d [L] is the mean stream depth, Qs [L^{3}T^{-1}] is stream discharge, I [L^{2}T^{-1}] is the rate of groundwater inflow, $^{222}Rn_{gw}$ [ML^{-3}] is the ^{222}Rn activity in the groundwater, k_{deg} [LT^{-1}] is the degassing coefficient derived from empirical functions (see [*Frei and Gilfedder*, 2015; *Unland et al.*, 2013; *Genereux and Hemond*, 1992]), λ_{Rn} [T^{-1}] the first order decay constant for ^{222}Rn, Q_r [L^{3}T^{-1}] is inflow from tributaries, R_L [L] the inflow length and $^{222}Rn_{trib}$ [ML^{-3}] the ^{222}Rn activity in tributaries. Reach specific parameters used for FINIFLUX simulations of the Vilqué catchment are listed in Table 2.

In Equation 11 α_1 [ML^{-1}T^{-1}] and α_2 [L^{2}T^{-1}] are reach specific parameters representing the enrichment and loss of in-stream ^{222}Rn due to hyporheic exchange. Both parameters can be derived by assuming that the hyporheic RT follow a pre-defined distribution model pdf_{RT} according to Equations 12 and 13 where γ [ML^{-3}T^{-1}] is the ^{222}Rn production rate (emanation rate) in the hyporheic sediments.

$$\alpha_1 = q_H\left[\frac{\gamma}{\lambda_{Rn}}\left(1 - \int_0^\infty e^{-\lambda_{Rn}\tau}\, pdf_{RT}(\tau)d\tau\right)\right] \quad (12)$$

$$\alpha_2 = -q_H\left[1 - \int_0^\infty e^{-\lambda_{Rn}\tau}\, pdf_{RT}(\tau)d\tau\right] \quad (13)$$

It is important to note that the hyporheic flux q_H, which is also needed for the quantification of hyporheic nitrate removal, does not include any interaction with regional groundwater flow consisting solely of infiltrating and exfiltrating stream water at steady state. This is identical to other commonly used hyporheic models such as OTIS and is a necessary simplification in the up-scaling process [*Runkel*, 1998]. The original version of FINIFLUX [*Frei and Gilfedder*, 2015] only supported an exponential distribution model for pdf_{RT}. As part of this study we additionally implemented power law and gamma-type pdf_{RT} models (Equations 8 and 9) to account for ^{222}Rn emanation in the HZ (modified version of FIIFLUX can be obtained from http://www.hydro.uni-bayreuth.de/hydro/en/software/software/software_dl.php?id_obj=129191).

By using the standard exponential pdf_{RT} Equations 11 and 12 can be solved analytically giving $\alpha_1 = \frac{\gamma\theta hw}{\lambda_{Rn}\tau_m + 1}$ and $\alpha_2 = -\frac{\theta\lambda_{Rn} hw}{\lambda_{Rn}\tau_m + 1}$ [*Cook*, 2013]. In the case of power law or a gamma distribution models the integrals in Equation 12 and 13 are solved numerically by using the adaptive quadrature techniques implemented in MATLAB. FINIFLUX is coupled to the automated parameter estimation software PEST [*Doherty et al.*, 1994] for model optimization. PEST is used to derive an objective function between the in-stream ^{222}Rn observations and numerical predictions, and depends on a set of pre-defined model parameters. Optimal parameter settings are systematically estimated within PEST targeting the best parameter set that minimizes the objective function. PEST estimates this optimal parameter set by applying the Gauss-Marquardt-Levenberg algorithm [*Doherty et al.*, 1994]. PEST coupling within FINIFLUX is set up to search for optimal groundwater inflow rates I and optimal hyporheic exchange parameters τ_m and h simultaneously.

3.2.2 Field case: Simulation of hyporheic nitrate removal

Hyporheic nitrate removal for the *Vilqué* catchment was simulated using the different pdf_{RT} models with the corresponding shape factors presented in Figure 2. In order to calculate the hyporheic water flux q_h (Equation 1), we used the mean hyporheic RT τ_m and the reach specific hyporheic exchange depths h that were estimated for every stream reach as part of the FINIFLUX simulation. For the representation of ET we used threshold factors derived from published reaction kinetics for aerobic respiration in the HZ (Table 3). Threshold factors based on 1st-order reaction kinetics for oxygen consumption for rippled streambeds as presented in *Kessler et al.* [2012] were derived by applying Equation 5. *Azizian et al.* [2015] have simulated aerobic respiration using a Monod rate expression for which a corresponding threshold factor was derived by applying Equation 6. Finally we also used a threshold value for '*a*' from literature that is based directly on field observations [*Gomez-Velez et al.*, 2015].

4. Results

4.1. Generic River Reach

In general for all pdf_{RT} scenarios the highest hyporheic nitrate removal efficiencies (13-72%) were achieved for simulations using a threshold factor of $a = 0$ hours (RT = ET) and low mean hyporheic RT (Figure 4 and 5).For gamma-type/exponential pdf_{RT} regions where $E \geq$ 3% (here the contour line E=3% was chosen only as an example to illustrate the sensitivity of simulated nitrate removal efficiencies) were equally found above and below the 1:1 line (Figure 4). By increasing the shape factor α_G areas where $E \geq 3\%$ were progressively shifted below the 1:1 line. Simulations using a power law pdf_{RT} obtained the highest modeled removal efficiencies ranging from 16 to 72% (Figure 5) Maximum simulated hyporheic nitrate removal efficiency for the generic river reach scenario of 72% was found for the power law pdf_{RT} with $\tau_m < 1$ hours, a shape factor of $\alpha_P = 1.2$ and a threshold factor of $a = 0$ hours. Contrary to

the gamma-type and exponential pdf_{RT} models (Figure 4), removal efficiencies rapidly decreased for the power law distributions at threshold factors $a > 0$ hours. For the power law pdf_{RT} regions of the graph where $E \geq 3\%$ only can be found below the $a = 0.5\tau_m$ line and an increase in the shape factor α_P further shifting the $E \geq 3\%$ bound towards lower τ_m values. In Figure 5 parts of the graph above the 1:1 line ($a = \tau_m$) are blanked as scaling factors A_r were close to zero subsequently resulting in a division by zero in Equation 2. The narrow range, where high hyporheic nutrient efficiencies can be achieved for simulations using power law pdf_{RT}, can be explained by the special shape of the distribution models (Figure 2). Compared to the gamma or exponential model, most of the power (area below the function) for power law pdf_{RT} is located at very low RT. Physically this can be interpreted as a system where majority of the flow paths are located in shallow areas of the HZ which are characterized by very low RT. For these shallow flow paths hyporheic nutrient removal is particularity high, which we will explain in detail later as part of chapter 4.4.2. If the shape factor α_P is increased more power is shifted towards low RT fractions in the pdf_{RT} (Figure 2). However if the threshold factor a is introduced these fractions associated with high hyporheic nitrate removal capacities (see chapter 4.4.2) are excluded and consequently removal rates and removal efficiencies are becoming lower (Figure 5).

4.2. Vilqué catchment

4.2.1 Groundwater Input and Hyporheic Exchange parameters

The ^{222}Rn activities in the *Vilqué* stream varied from <100 to 16,000 Bq m^{-3} (Figure 6). The first 350 m of the stream showed ^{222}Rn activities with values below 100 Bq m^{-3}. Prior to the first sampling point the stream flows down an escarpment (Figure 3D) which produces highly turbulent conditions and high radon degassing which can account for the low ^{222}Rn activities.

At *x = 360 m* the ^{222}Rn activity rapidly increased from ~ 100 Bq m^{-3} to 16,000 Bq m^{-3} indicating a point source of groundwater discharge. An inflowing spring was identified on the stream bank with a ^{222}Rn activity of 52,000 Bq m^{-3} (Figure 6A). This value was used as the groundwater end-member ($^{222}Rn_{gw}$ in Equation 11) as part of the FINIFLUX simulations. It is also likely that groundwater entered the stream through the streambed, and the spring is only a visual indicator for the upwelling of deeper groundwater. A second local maximum in ^{222}Rn activity of ≈ 5,000 Bq m^{-3} was measured at *x = 1,946 m*, indicating a second stream reach that was preferentially influenced by groundwater inflow. Stream discharge rapidly increased for the first stream kilometer, especially in the area around the spring. For reaches located further downstream (between 1.5 km and 2 km), close to the catchment's outlet, discharge slightly decreased. The highest nitrate concentrations were measured in the upstream areas of the catchment (45 mg l^{-1}) and decreased to ≈ 31 mg l^{-1} towards the catchment's outlet. The inverse correlation between measured nitrate concentrations and discharge suggests that nitrate was diluted by inflowing ground or surface water and nitrate loss due to hyporheic nitrate removal processes (Figure 6B).

^{222}Rn and stream discharge were used to quantify groundwater inflow and hyporheic exchange parameters as part of the FINIFLUX simulations. For all scenarios modeled ^{222}Rn activities were close to the observed values with a correlation coefficient of ≈ 0.997 (a selection of three different distribution models are shown in Figure 6A). On average the different pdf_{RT} scenarios systematically were overestimating the observed ^{222}Rn activities by ~480 Bq m^{-3}. The highest discrepancy between modeled and measured ^{222}Rn activities was 1,300 Bq m^{-3} (8%) and is located where the spring enters the stream. Maximum difference in the simulated ^{222}Rn activities for the different pdf_{RT} scenarios, with ~20 Bq m^{-3} lie close to the detection limit (15 Bq m^{-3}) and were considered as insignificant (Figure 6A-D). The groundwater

influxes for the stream reaches upstream of the spring were close to zero for all scenarios (Figure 6D). At the spring location (*x = 360 m*) the modeled groundwater inflow was 1.7×10^{-3} $m^3 s^{-1}$. For the reach where the second ^{222}Rn peak (*x = 1946 m*) is located the groundwater inflow was estimated at ~0.6×10^{-3} $m^3 s^{-1}$. For the entire 2.3 km of the stream the groundwater inflow for the different scenarios varied between 5.52×10^{-3} and 5.54×10^{-3} $m^3 s^{-1}$ (Figure 6D). The net increase in measured stream discharge between the first and the last measuring point was 9.3×10^{-3} $m^3 s^{-1}$ which suggests that the modeled groundwater component makes up approximately 60% of the change in stream flow over the 2.3 km catchment. The remaining 40% (3.8×10^{-3} $m^3 s^{-1}$) likely comes from small farm drains and ditches which were observed in the field but not quantified.

Among the different distribution models pdf_{RT}, inversely estimated τ_m were almost identical and varied from 2.4 to 2.6 hours (Figure 6C and D). The highest τ_m and the highest variability in τ_m came from the power law pdf_{RT}. The cumulated hyporheic water flux for the entire 2.3 km of the stream was ~18×10^{-3} $m^3 s^{-1}$ with only very little difference between the various pdf_{RT} models (Figure 6D). This suggests that more than half of the stream water passes through the HZ at some point over the 2.4 km, which is consistent with other hyporheic studies on small streams [*Liao et al.*, 2013]. For the last two stream reaches groundwater input and hyporheic exchange was close to zero, which is also consistent with field observations as the streambed in this area was characterized by a high clay content preventing hyporheic exchange as well as very field data showing little change, or even a decrease, in discharge.

4.2.2 Hyporheic Nitrate Removal

Hyporheic nitrate removal was simulated using the estimated hyporheic exchange parameters from the FINIFLUX simulations and measured stream nitrate concentrations C_{in}. Hyporheic nitrate removal was simulated for all pdf_{RT} models by 1) assuming that hyporheic RT are equal to the ET ($pdf_{RT} = pdf_{ET}$) which means that nitrate processing starts as soon as stream water enters the hyporheic zone ($a = 0$) and 2) that there is a distinct difference between RT and ET where $pdf_{RT} \neq pdf_{ET}$ by introducing the different threshold factors discussed above. In Figure 7 the spatial development of hyporheic nitrate turnover is shown for three different pdf_{RT} scenarios (exponential, α_G=0.5, α_P=1). Although absolute values for simulated hyporheic nutrient turnover did vary among the different pdf_{RT} scenarios, all models had in common that hyporheic removal rates for the last two stream reaches were close to zero. The reason for this was the almost zero hyporheic flux q_H for the last two stream reaches suggested by the FINIFLUX simulations (Figure 6D). Among the three different scenarios, highest hyporheic nitrate removal was simulated by setting a=0 hours for the power law distribution (0.33 kg h^{-1}), followed by the gamma (0.21 kg h^{-1}) and exponential (0.20 kg h^{-1}) distribution models (Figure 7A). By assuming $ET \neq RT$ and using a threshold factor $a > 0$, hyporheic nitrate removal was significantly reduced (Figure 7A). For $a = 2.3$ hours (Figure 7) hyporheic nitrate removal for the entire stream decreased to 0.11 kg h^{-1} for the gamma model, 0.09 kg h^{-1} for the exponential model and 0.01 kg h^{-1} for the power law model. This is a reduction of 48-97 %.

Total hyporheic nitrate removal and removal efficiencies for all simulated pdf_{RT} scenarios are shown in Figure 8. Hyporheic nitrate removal efficiencies were calculated according to Equation 10 by setting the parameters in the denominator to corresponding values estimated for the catchments outlet at the last stream reach (C_{in} = 31.06 mg L^{-1} and Q_s = 0.012 m^3 s^{-1}). For

all simulations performed for the *Vilqué* (Figure 8), and as found in the generic river reach scenarios, simulations using power law distribution models resulted in both the highest and lowest hyporheic nitrate removal and removal efficiencies depending on whether pdf_{RT} or pdf_{ET} were used. This is due to the particular shape of the power law distribution (Figure 2). Compared to the gamma and exponential models most of the weight (area below the distribution) of the power law distribution is located at very short RT. This physically can be interpreted as shallow flow paths in the HZ with low hyporheic RT and a large hyporheic water flux q_h. For these flow paths, the relative change in nitrate concentration (C_{in} - C_{out}) is low. However, mass removal scales with the hyporheic water flux, which is highest in the shallow areas of the HZ. These areas are removed from the power law distribution by introducing a threshold factor $a > 0$, with only the tail of the power law distribution contributing to the reactive part of the hyporheic water flux q_{ET} and thus hyporheic nitrate removal. This can be seen when comparing the average q_{ET} for the three different distribution models (Figure 7) where q_{ET} for the power law distribution (0.0014 $m^3\ m^{-1}\ h^{-1}$) is considerably lower compared to the gamma (0.009 $m^3\ m^{-1}\ h^{-1}$) and exponential (0.011 $m^3\ m^{-1}\ h^{-1}$) models.

5. Discussion

In the HZ the complex interplay between hydrodynamic flow and redox-sensitive biogeochemical reactions creates conditions where nitrogen is non-uniformly processed [*Frei et al.*, 2018]. Heterotrophic and autotrophic hyporheic nitrate removal pathways are capable of permanently and/or temporarily removing nitrogen from fluvial systems [*Burgin and Hamilton*, 2007]. In the LPM presented here, the primary controls on hyporheic nitrate removal are only represented in a simplified manner compared to real world conditions. We assume that the various processes responsible for hyporheic nitrate removal can be represented in a lumped fashion using a single kinetic expression that hinges on the absence of oxygen. In reality, stream reaches can also be net nitrate sources [*Zarnetske et al.*, 2012; *Briggs et al.*, 2014] through nitrification, where ammonium originating either from incomplete hyporheic nitrate removal pathways (e.g. DNRA) or aerobic respiration are oxidized to nitrate. This is currently unaccounted for in the presented LPM, in that we assume that the HZ acts solely as a permanent sink for nitrogen. Processes such as nitrification would reduce the net efficiency of streams to remove nitrate, and thus our estimates may be an upper limit to nitrate loss in the HZ. Also we do not account for mixing processes with local groundwater in the HZ nor the suppressing effect of inflowing groundwater on hyporheic exchange [*Trauth et al.*, 2013]. Streambed heterogeneity can have an important influence on hyporheic exchange characteristics [*Pryshlak et al.*, 2015], hyporheic residence times [*Tonina et al.*, 2016] and can be responsible for the formation of biogeochemical hot spots [*Gomez-Velez et al.*, 2014]. By treating the HZ as box containing homogenous streambed materials where characteristics of transport are represented in a lumped fashion some of the aspects relevant under real world conditions cannot be accounted for in the LPM. The benefit associated with this high level of abstraction is the ability to upscale complex hydrological and biogeochemical processes to river reaches or entire catchments with a minimal number of parameters and computer power.

Compared to spatially explicit process-based model structures [*Gomez-Velez et al.*, 2015] LPM usually do not need the level of detail required to set up and run flow and transport simulations.

The concept presented as part of this study is based on the fundamental idea that there exists a distinct relationship between pdf_{RT} and pdf_{ET} in non-well mixed hydrological systems [*Frei and Peiffer*, 2016]. The a-priori choice of 1) a suitable analytical distribution model to represent hyporheic RT and 2) a threshold factor that defines the time scales over which hyporheic nitrate removal processes are suppressed by the presence of oxygen are the critical components in the LPM. A similar LPM was used by *Pittroff et al.* [2017] in order to quantify the hyporheic nitrate removal for a 32 km long river reach of the Roter Main River in South-East Germany. Despite considerable oxygen levels in the hyporheic sediments [*Pittroff et al.*, 2017], the authors still assumed that hyporheic nitrate removal was initiated as soon as stream water entered the subsurface. This assumption is identical to our simulations scenarios where the threshold factor $a = 0$. Moreover, the simulations in *Pittroff et al.* [2017] were carried out using exclusively an exponential model for hyporeic residence times (pdf_{RT}). As shown for the generic river reach and the *Vilqué* catchment, the combination of different distribution models and threshold factors can lead to very different estimates for hyporheic nitrate removal. In particular simulations that use power law models show very inefficient hyporheic nitrate removal as soon as the threshold factor approaches the mean hyporheic RT. This is significant as power law distributions are often associated with hydrological systems [*Kirchner et al.*, 2000; *Kollet and Maxwell*, 2008b] including the HZ [*Haggerty et al.*, 2002].

For the *Vilqué* catchment nutrient removal was estimated based on hyporheic parameters that are originated from inverse ^{222}Rn mass balance modeling using the FINIFLUX model. Here we explicitly note that the LPM framework does not necessarily require a ^{222}Rn mass balance

with the only prerequisite being some way to estimate a mean hyporheic RT and hyporheic exchange depth *h* for a given pdf_{RT}. For ^{222}Rn mass balance modeling, the specific type of pdf_{RT} model used to describe enrichment of ^{222}Rn in the hyporheic zone seems to be of minor importance. This can be attributed to the main source of stream ^{222}Rn stemming from groundwater discharge due to its high ^{222}Rn signature. Enrichment of stream water with ^{222}Rn due to hyporheic flow only seems to play a subordinate role in this case due to the shallow hyporheic depth and narrow stream width. However, this also may be related with to the fact that the applied longitudinal stream ^{222}Rn mass balance was reported to be insensitive to hyporheic zone residence times of below a few days [*Cook*, 2013].

For hyporheic nitrate removal the choice of a pdf_{RT} model is important and can lead to significantly different results depending on which pdf_{RT} is used. This was particularly evident for power law pdf_{RT} where mass loss was up to 33% higher than either the gamma or exponential functions for $a = 0$ but approached zero when ETs were included in the calculations. These findings indicate that hyporheic systems can be very inefficient in removing nitrate especially when oxygen availability is high for parts of the pdf_{RT} where most of the hyporheic water flux occurs. Although hyporheic nitrate removal can be minimal for the shallow aerobic areas the presence of oxygen can facilitate nitrification up to a point where the HZ is a net-source for nitrate [*Briggs et al.*, 2014; *Zarnetske et al.*, 2012].

Catchment wide input-output mass balances are often associated with a high uncertainty. However, they can be a useful test of the plausibility of model results and to identify possible inconsistencies with observations. For the *Vilqué* stream we calculated a nitrate input to the uppermost reach of 9.6 kg d^{-1} and at the outlet a flux of 31.7 kg d^{-1}. By using the mean groundwater flux from these three scenarios and the nitrate concentration in the spring, the nitrate flux from the aquifer into the stream can be quantified at 14.3 kg d^{-1}. Hyporheic nitrate

removal in the HZ varied significantly depending on which pdf_{RT} model was used and whether the ET method was applied or not. Maximum hyporheic nitrate removal (10.8 kg d^{-1}) was calculated using the power law distribution model with a shape factor of $\alpha_p = 1.2$ and $a = 0$. For all pdf_{RT} models, minimum and near zero mass removal occurred at a threshold factor of $a = 4.2$ hours. This leaves an unaccounted nitrate source in the mass-balance ranging from 7.8 - 18.6 kg d^{-1}. For the *Vilqué* catchment we assume that the missing nitrate flux originates from the unaccounted water source associated with surface or near surface inflows due to drains and ditches that were not quantified during the field campaign. Theoretically this unaccounted component can be represented as part of the FINFLUX simulation via the tributary input term (Equation 11). This however would require defining the specific location where surface flow from drains is entering the stream which is difficult for a more diffuse water source that cannot be localized exactly. As the parameters obtained from FINIFLUX used to quantify hyporheic nitrate removal (q_h, h and τ_m) are quite robust for the different FININFLUX scenarios, we think the outcome in terms of the estimated hyporheic nitrate removal rates would be very similar by accounting for the missing drainage water. By dividing the missing water flux (3.8×10^{-3} m^3 s^{-1}) by the range of unaccounted nitrate flux 7.8 - 18.7 kg d^{-1}, an expected nitrate concentrations in the drain end member can be estimated for the different pdf_{RT} scenarios (Figure 9). This can then be compared to the variability of measured stream nitrate concentrations. Two scenarios simulated for the power law pdf_{RT} model produce estimated drain nitrate concentrations lying above the 75 percentile of measured instream nitrate concentrations and can probably be excluded as realistic. Nitrate concentration in the drains should lie close to or below to the ones measured in the stream as observations (Figure 6) suggest that nitrate is diluted by inflowing water from the drains. All the other scenarios produce nitrate concentrations lying in a plausible range. For the gamma-type and exponential pdf_{RT}, almost all concentrations are lying within the 25 (32 mg l^{-1}) -75 (44 mg l^{-1}) percentiles

of measured stream nitrate concentrations. The scenarios that come closest to the median stream water concentration use gamma-type pdf_{RT} with a shape factor of $\alpha_p > 0.1$ and a threshold factor of a = 0.35 hours. For the *Vilqué* catchment improved nitrate mass balances could be achieved by further narrowing the uncertainties associated with the FINIFLUX simulations and the parameterization of the ET. This would require additional field measurements to constrain hyporheic exchange depths, measurements (e.g. N_2-emission) to directly quantify denitrification in the HZ or in-situ oxygen measurements that can be used to derive an appropriate threshold factor for each reach.

6. Conclusions

Quantification of nutrient removal associated with natural degradation and transformation in managed and unmanaged catchments is a major challenge in environmental science. The framework presented here is a simple way to combine hydrological transport and biogeochemical reactions using a LPM. The concept can be incorporated into existing tracer modeling routines such as OTIS [*Runkel*, 1998] when simulating reactive transport processes in storage zones. It is one of the few methods that can be applied to estimate hyporheic nitrate removal on scales of river networks and catchments. By incorporating ET to account for the effective timescales of biogeochemical reaction in the HZ, modeled removal efficiencies decrease dramatically compared to scenarios where RT are assumed to represent the time scale available for reaction. We conclude that ET will likely lead to more realistic estimates for nutrient removal in hyporheic systems.

Acknowledgments

This research was supported in part by the Loire Brittany Water agency (AELB), the Franco-Bavarian University cooperation center BayFrance (www.bayern-france.org/en/) and the German Research Foundation (DFG) project number FR 2858/2-1-3013594. It was also supported by the internal funds of the Limnological Research Station, Bayreuth. The authors thank Christian Camerlynck for the seismic cross section and the anonymous reviewers for their helpful comments. Data to this manuscript can be downloaded from http://www.hydro.uni-bayreuth.de/hydro/de/software/software/software_dl.php?id_obj=151411

References

Azizian, M., S. B. Grant, A. J. Kessler, P. L. M. Cook, M. A. Rippy, and M. J. Stewardson (2015), Bedforms as biocatalytic filters: A pumping and streamline segregation model for nitrate removal in permeable sediments, *Environmental Science & Technology*, *49*(18), 10993–11002.

Boano, F., J. W. Harvey, A. Marion, A. I. Packman, R. Revelli, L. Ridolfi, and A. Wörman (2014), Hyporheic flow and transport processes: Mechanisms, models, and biogeochemical implications, *Reviews of Geophysics*.

Briggs, M. A., L. K. Lautz, and D. K. Hare (2014), Residence time control on hot moments of net nitrate production and uptake in the hyporheic zone, *Hydrol. Process*, *28*(11), 3741–3751.

Burgin, A. J., and S. K. Hamilton (2007), Have we overemphasized the role of denitrification in aquatic ecosystems? A review of nitrate removal pathways, *Frontiers in Ecology and the Environment*, *5*(2), 89–96.

Cann, C. (1998), Evolution de l'agriculture et de sa pression polluante sur le bassin et en Bretagne, *C. Cheverry Agriculture intensive et qualit édes eaux INRA Paris*, 25–40.

Cardenas, M. B., J. L. Wilson, and V. A. Zlotnik (2004), Impact of heterogeneity, bed forms, and stream curvature on subchannel hyporheic exchange, *Water Resources Research*, *40*(8).

Cartwright, I., A. P. Atkinson, B. S. Gilfedder, H. Hofmann, D. I. Cendón, and U. Morgenstern (2018), Using geochemistry to understand water sources and transit times in headwater streams of a temperate rainforest, *Applied Geochemistry*.

Cartwright, I., and B. Gilfedder (2015), Mapping and quantifying groundwater inflows to Deep Creek (Maribyrnong catchment, SE Australia) using 222Rn, implications for protecting groundwater-dependant ecosystems, *Applied Geochemistry*, *52*, 118–129.

Cook, P. G. (2013), Estimating groundwater discharge to rivers from river chemistry surveys, *Hydrological Processes*, *27*(25), 3694–3707.

Doherty, J., L. Brebber, and P. Whyte (1994), PEST: Model-independent parameter estimation, *Watermark Computing, Corinda, Australia*, *122*.

Fowler, D., M. Coyle, U. Skiba, M. A. Sutton, J. N. Cape, S. Reis, L. J. Sheppard, A. Jenkins, B. Grizzetti, and J. N. Galloway (2013), The global nitrogen cycle in the twenty-first century, *Philosophical Transactions of the Royal Society of London. B, Biological Sciences*, *368*(1621), 20130164.

Frei, S., M. Azizian, S. B. Grant, V. A. Zlotnik, and D. Toundykov (2018), Analytical modeling of hyporheic flow for in-stream bedforms: Perturbation method and implementation, *Environmental Modelling & Software*, doi:10.1016/j.envsoft.2018.09.015.

Frei, S., and B. S. Gilfedder (2015), FINIFLUX: An implicit finite element model for quantification of groundwater fluxes and hyporheic exchange in streams and rivers using radon, *Water Resources Research*, *51*(8), 6776–6786.

Frei, S., and S. Peiffer (2016), Exposure times rather than residence times control redox transformation efficiencies in riparian wetlands, *Journal of Hydrology*, *543*, 182–196.

Galloway, J. N., F. J. Dentener, D. G. Capone, E. W. Boyer, R. W. Howarth, S. P. Seitzinger, G. P. Asner, C. C. Cleveland, P. A. Green, and E. A. Holland (2004), Nitrogen cycles: past, present, and future, *Biogeochemistry*, *70*(2), 153–226.

Genereux, D. P., and H. F. Hemond (1992), Determination of gas exchange rate constants for a small stream on Walker Branch Watershed, Tennessee, *Water Resour. Res.*, *28*(9), 2365–2374.

Ginn, T. R. (1999), On the distribution of multicomponent mixtures over generalized exposure time in subsurface flow and reactive transport: Foundations, and formulations for groundwater age, chemical heterogeneity, and biodegradation, *Water Resources Research*, *35*(5), 1395–1407.

Gomez-Velez, J. D., J. W. Harvey, M. B. Cardenas, and B. Kiel (2015), Denitrification in the Mississippi River network controlled by flow through river bedforms, *Nature Geoscience*, *8*(12), 941–945.

Gomez-Velez, J. D., S. Krause, and J. L. Wilson (2014), Effect of low-permeability layers on spatial patterns of hyporheic exchange and groundwater upwelling, *Water Resour. Res.*, *50*(6), 5196–5215.

Gu, C., W. Anderson, and F. Maggi (2012), Riparian biogeochemical hot moments induced by stream fluctuations, *Water Resour. Res.*, *48*(9).

Haase, P., J. D. Tonkin, S. Stoll, B. Burkhard, M. Frenzel, I. R. Geijzendorffer, C. Häuser, S. Klotz, I. Kühn, and W. H. McDowell (2018), The next generation of site-based long-term ecological monitoring: linking essential biodiversity variables and ecosystem integrity, *Science of the Total Environment*, *613*, 1376–1384.

Haggerty, R., S. M. Wondzell, and M. A. Johnson (2002), Power-law residence time distribution in the hyporheic zone of a 2nd-order mountain stream, *GEOPHYSICAL RESEARCH LETTERS*, *29*(13), 1640.

Hespanha, J. P. (2018), *Linear systems theory*, 2nd ed., 330 pp., Princeton University Press, Princeton and Oxford.

Kessler, A. J., R. N. Glud, M. B. Cardenas, and P. L. M. Cook (2013), Transport zonation limits coupled nitrification-denitrification in permeable sediments, *Environmental Science & Technology*, *47*(23), 13404–13411.

Kessler, A. J., R. N. Glud, M. B. Cardenas, M. Larsen, M. F. Bourke, and P. L. M. Cook (2012), Quantifying denitrification in rippled permeable sands through combined flume experiments and modeling, *Limnology and Oceanography*, *57*(4), 1217–1232.

Kiel, B. A., and M. B. Cardenas (2014), Lateral hyporheic exchange throughout the Mississippi River network, *Nature Geoscience*, *7*(6), 413.

Kirchner, J. W., X. Feng, and C. Neal (2000), Fractal stream chemistry and its implications for contaminant transport in catchments, *Nature*, *403*(6769), 524–527, doi:10.1038/35000537.

Kollet, S. J., and R. M. Maxwell (2008b), Demonstrating fractal scaling of baseflow residence time distributions using a fully-coupled groundwater and land surface model, *GEOPHYSICAL RESEARCH LETTERS*, *35*(7), 7402.

Lee, J.-M., and G. Kim (2006), A simple and rapid method for analyzing radon in coastal and ground waters using a radon-in-air monitor, *Journal of environmental radioactivity*, *89*(3), 219–228.

Liao, Z., D. Lemke, K. Osenbrück, and O. A. Cirpka (2013), Modeling and inverting reactive stream tracers undergoing two-site sorption and decay in the hyporheic zone, *Water Resources Research*, *49*(6), 3406–3422.

Lohse, K.A., P.D. Brooks, J.C. McIntosh, T. Meixner, and T.E. Huxman (2009), Interactions between biogeochemistry and hydrologic systems, *Annual Review of Environment and Resources*, *34*, 65–96.

Małoszewski, P., and A. Zuber (1982), Determining the turnover time of groundwater systems with the aid of environmental tracers: 1. Models and their applicability, *Journal of Hydrology(Amsterdam)*, *57*(3-4), 207–231.

Marzadri, A., D. Tonina, and A. Bellin (2012), Morphodynamic controls on redox conditions and on nitrogen dynamics within the hyporheic zone: Application to gravel bed rivers with alternate-bar morphology, *Journal of Geophysical Research: Biogeosciences*, *117*(G3).

Mirtl, M., E. T. Borer, I. Djukic, M. Forsius, H. Haubold, W. Hugo, J. Jourdan, D. Lindenmayer, W. H. McDowell, and H. Muraoka (2018), Genesis, goals and achievements of long-term ecological research at the global scale: a critical review of ILTER and future directions, *Sci. Total Environ*, *626*, 1439–1462.

Morgenstern, U., M. K. Stewart, and R. Stenger (2010), Dating of streamwater using tritium in a post nuclear bomb pulse world: continuous variation of mean transit time with streamflow, *Hydrology and Earth System Sciences*, *14*(11), 2289–2301.

Oldham, C. E., D. E. Farrow, and S. Peiffer (2013), A generalized Damkohler number for classifying material processing in hydrological systems, *Hydrology and Earth System Sciences*, *17*(3), 1133.

Pittroff, M., S. Frei, and B. S. Gilfedder (2017), Quantifying nitrate and oxygen reduction rates in the hyporheic zone using 222Rn to upscale biogeochemical turnover in rivers, *Water Resources Research*, *53*(1), 563–579.

Pryshlak, T. T., A. H. Sawyer, S. H. Stonedahl, and M. R. Soltanian (2015), Multiscale hyporheic exchange through strongly heterogeneous sediments, *Water Resour. Res.*, *51*(11), 9127–9140.

Rantz, S. E. (1982), Measurement and computation of streamflow: Volume 1, Measurement of stage and discharge, *WATER-SUPPLY PAPER 2175*, USGS, Washington D.C.

Runkel, R. L. (1998), One-dimensional transport with inflow and storage (OTIS): A solute transport model for streams and rivers, US Department of the Interior, US Geological Survey.

Sanz-Prat, A., C. Lu, R. T. Amos, M. Finkel, D. W. Blowes, and O. A. Cirpka (2016), Exposure-time based modeling of nonlinear reactive transport in porous media subject to physical and geochemical heterogeneity, *Journal of contaminant hydrology*, *192*, 35–49.

Schlesinger, W. H. (2004), Better living through biogeochemistry, *Ecology*, *85*(9), 2402–2407.

Seeboonruang, U., and T. R. Ginn (2006), Upscaling heterogeneity in aquifer reactivity via exposure-time concept: Forward model, *Journal of contaminant hydrology*, *84*(3), 127–154.

Thomas, Z., B. W. Abbott, O. Troccaz, J. Baudry, and G. Pinay (2016), Proximate and ultimate controls on carbon and nutrient dynamics of small agricultural catchments, *Biogeosciences*, *13*(6), 1863–1875, doi:10.5194/bg-13-1863-2016.

Thomas, Z., P. Rousseau-Gueutin, B. W. Abbott, T. Kolbe, H. Le Lay, J. Marçais, F. Rouault, C. Petton, P. Pichelin, and G. Le Hennaff (2019), Long-term ecological observatories needed to understand ecohydrological systems in the Anthropocene: a catchment-scale case study in Brittany, France, *Regional Environmental Change*, *19*(2), 363–377.

Tonina, D., F. P. J. de Barros, A. Marzadri, and A. Bellin (2016), Does streambed heterogeneity matter for hyporheic residence time distribution in sand-bedded streams?, *Advances in Water Resources*, *96*, 120–126.

Trauth, N., C. Schmidt, U. Maier, M. Vieweg, and J. H. Fleckenstein (2013), Coupled 3-D stream flow and hyporheic flow model under varying stream and ambient groundwater flow conditions in a pool-riffle system, *Water Resources Research*, *49*(9), 5834–5850.

Trauth, N., C. Schmidt, M. Vieweg, U. Maier, and J. H. Fleckenstein (2014), Hyporheic transport and biogeochemical reactions in pool-riffle systems under varying ambient groundwater flow conditions, *Journal of Geophysical Research: Biogeosciences*, *119*(5), 910–928.

Unland, N. P., I. Cartwright, G. C. Rau, J. Reed, B. S. Gilfedder, A. P. Atkinson, and H. Hofmann (2013), Investigating the spatio-temporal variability in groundwater and surface water interactions: a multi-technique approach, *Hydrology and Earth System Sciences*, *17*(9), 3437.

Vieweg, M., M. J. Kurz, N. Trauth, J. H. Fleckenstein, A. Musolff, and C. Schmidt (2016), Estimating time-variable aerobic respiration in the streambed by combining electrical conductivity and dissolved oxygen time series, *Journal of Geophysical Research: Biogeosciences*, *121*(8), 2199–2215.

Zarnetske, J. P., R. Haggerty, S. M. Wondzell, and M. A. Baker (2011), Dynamics of nitrate production and removal as a function of residence time in the hyporheic zone, *Journal of Geophysical Research: Biogeosciences*, *116*(G1).

Zarnetske, J. P., R. Haggerty, S. M. Wondzell, V. A. Bokil, and R. González-Pinzón (2012), Coupled transport and reaction kinetics control the nitrate source-sink function of hyporheic zones, *Water Resources Research*, *48*(11).

Table 1: Parameterization of the generic river reach used to quantify hyporheic nutrient removal for different parameter combinations of a and τ_m and different RT distribution models.

N reaches [-]	1
w [m]	1.0
h [m]	0.25
Θ [-]	0.4
τ_m [h]	0-30
a [h]	0-30
Q_s [$m^3\ s^{-1}$]	1
Δx [m]	100
Cin [$g\ m^{-3}$]	40

Table 2: Reach specific values for the FINIFLUX simulations used for the Vilqué catchment.

N observations [-]	14
N reaches [-]	13
$^{222}Rn_{gw}$ [Bq m^{-3}]	52,000
w [m]	0.22-0.78
d [m]	0.011-0.169
h [m]	0.001-0.570 (PEST calibrated)
Θ [-]	0.4
τ_m [h]	2.4-2.6 (PEST calibrated)
a [h]	Table 3
I [m^3 m^{-1} s^{-1}]	2.6x10^{-8} - 5x10^{-5} (PEST calibrated)
Q_s [m^3 s^{-1}]	2.5-12.8x10^{-3}
Q_R [m^3 s^{-1}]	0
R_L [m]	0
$^{222}Rn_{trib}$ [Bq m^{-3}]	0
Δx [m]	16-419

Table 3: Threshold factors used to simulate hyporheic nitrate removal of the stream Vilqué.

Reaction kinetics	Threshold factor *a* [h]	Reference
ET = RT	0	-
First order	0.35	*Kessler et al.* [2012]
Field observations	1	*Gomez-Velez et al.* [2015]
First order	1.6	*Kessler et al.* [2012]
Monod-type (95% criterion)	2.3	modified after *Azizian et al.* [2015]
Monod-type (using inhibitor criterion)	4.2	*Azizian et al.* [2015]

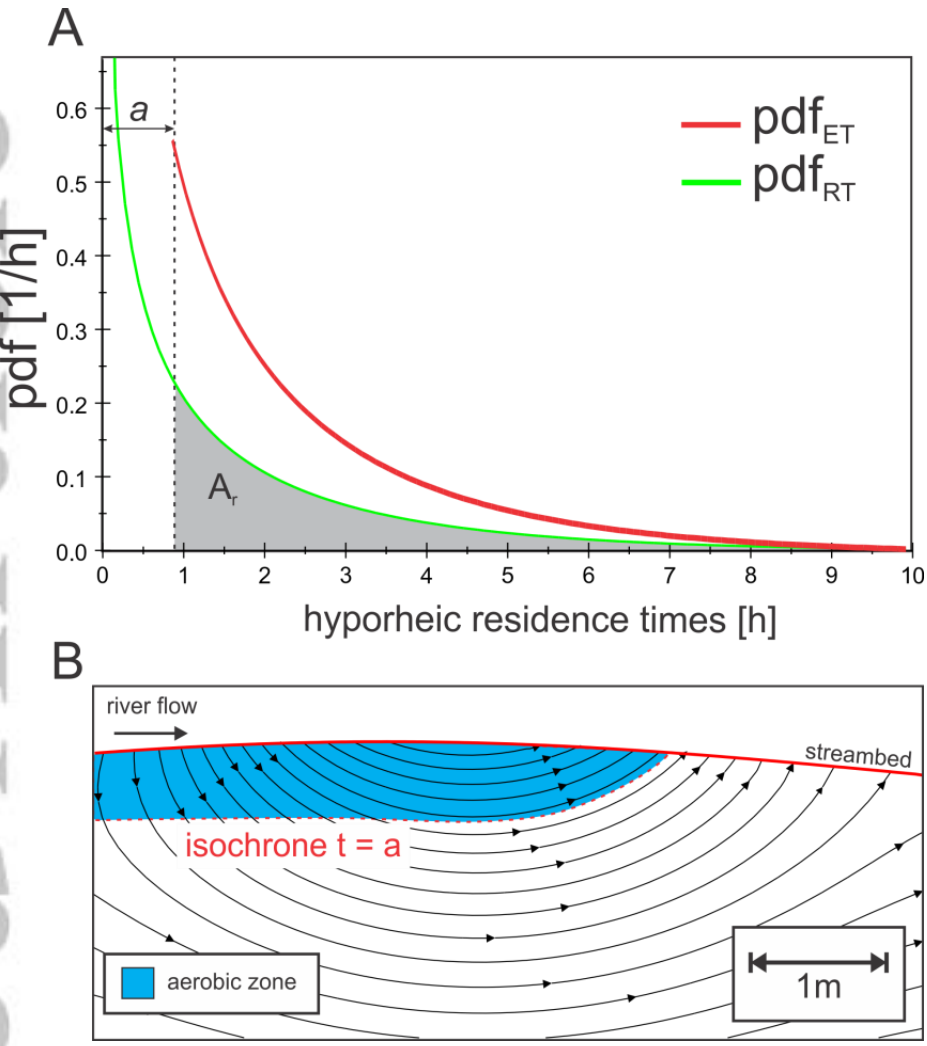

Figure 1: Deriving a *pdf*$_{ET}$ from a *pdf*$_{RT}$ by introducing the threshold factor *a.* 'a' represents the lag time prior to hyporheic nitrate removal caused by the inhibiting presence of oxygen. An exponential distribution model was used for visualization of the underlying concept.

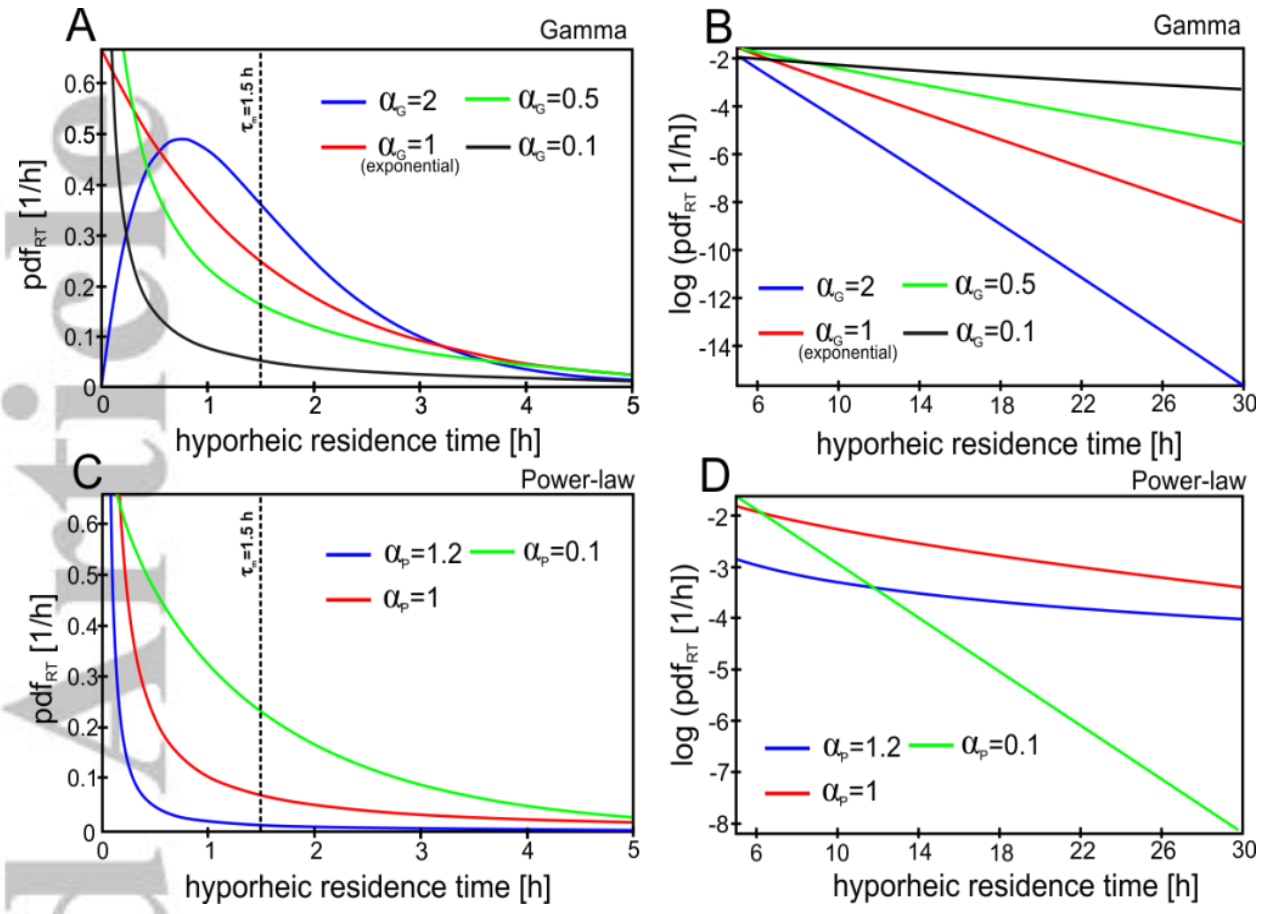

Figure 2: Various types of pdf_{RT} models used for the generic river reach scenario. All pdf_{RT} have a common mean value of τ_m = 1.5 hours. Plot A+B: Gamma-Type distribution models for different values of α_G (tail behavior of the distributions are shown in plot B). Plot C+D: Power-law with exponential cutoff distribution models for different values of α_P (tail behavior of the distributions are shown in plot D).

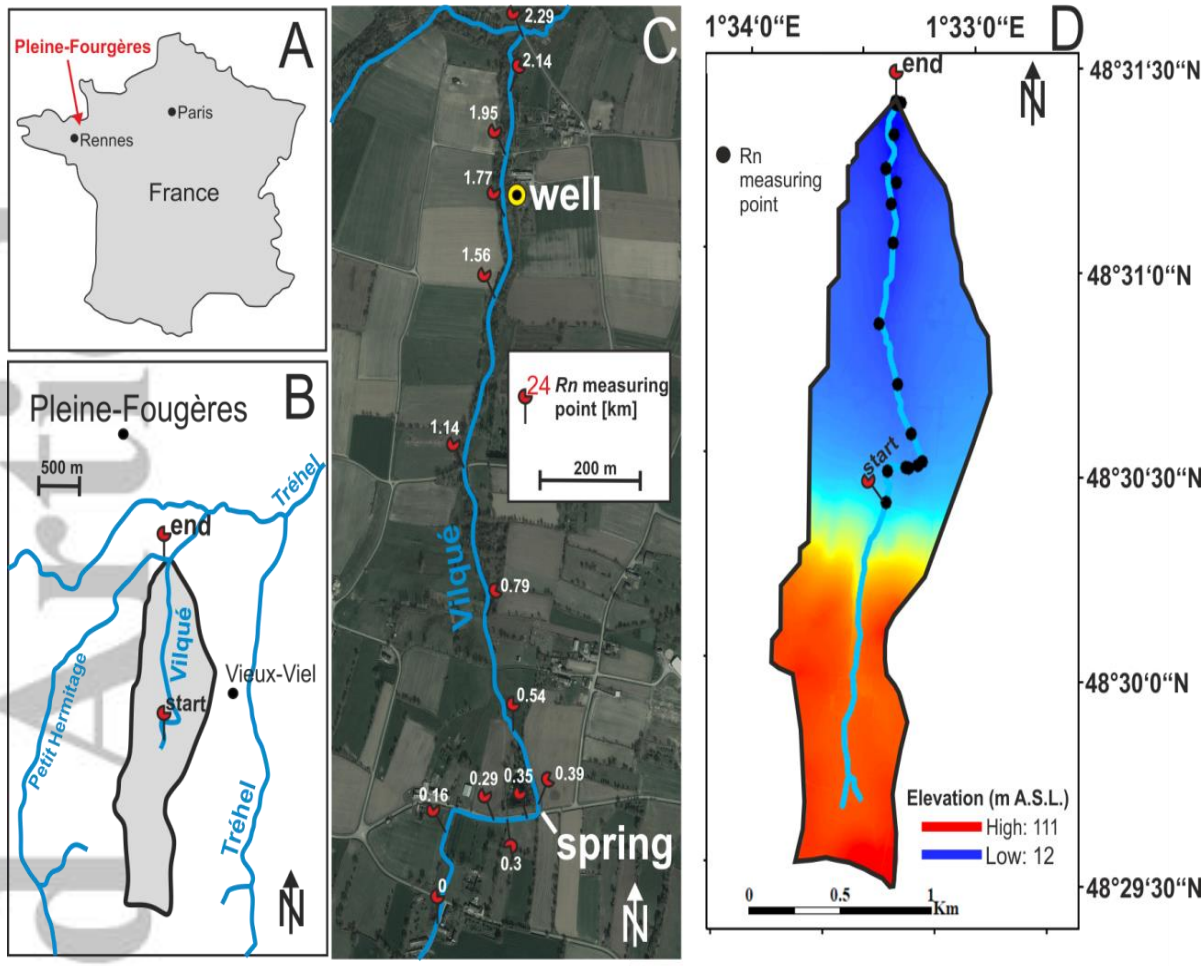

Figure 3: A-C) Location of the surveyed stream section at the ZAAr (Zone Atelier Armorique), Long-Term Socio-ecological Research platform (LTSER) located in the northwest of France near the town of Pleine–Fougères. D) Digital elevation model (DEM) of the Villqué catchment.

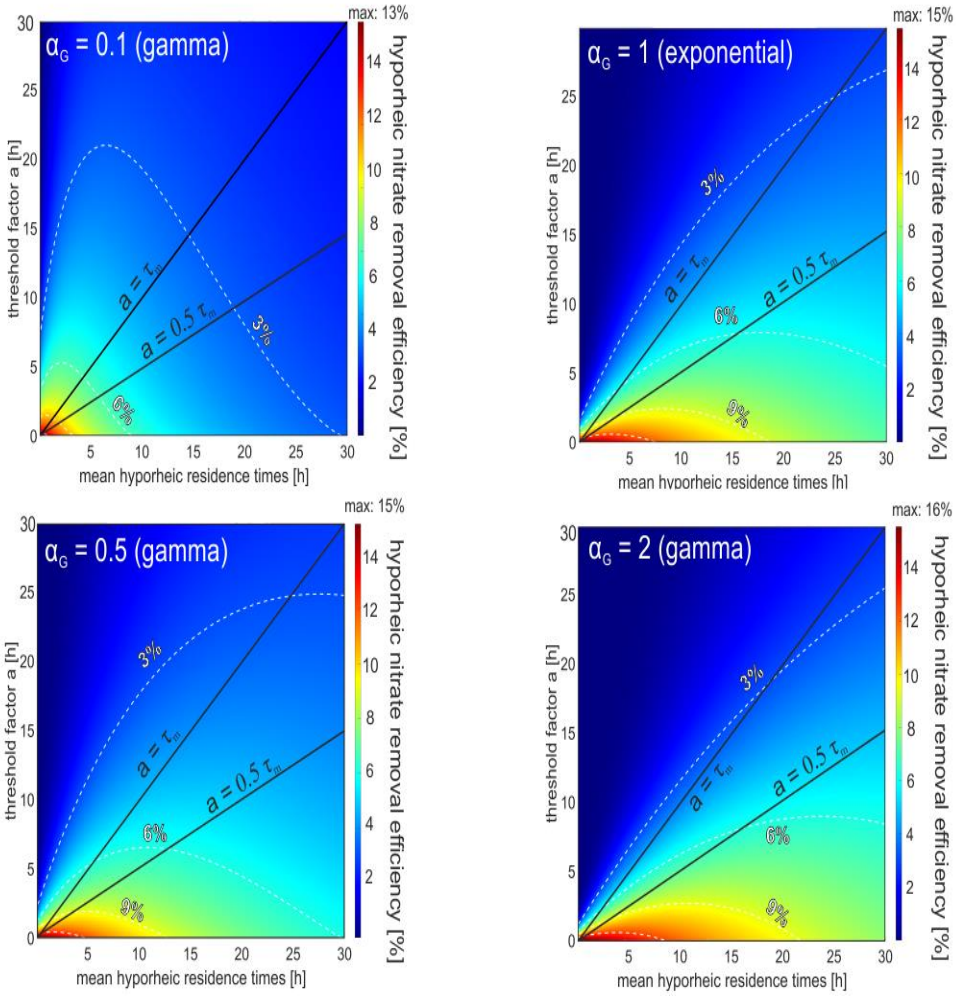

Figure 4: Simulated hyporheic nitrate removal efficiencies for the generic river reach using different parameter sets for mean resident times τ_m, threshold factors a and shape factors α_G for gamma-type RT distribution models. Note where the gamma parameter α_G is 1 it is equal to an exponential distribution.

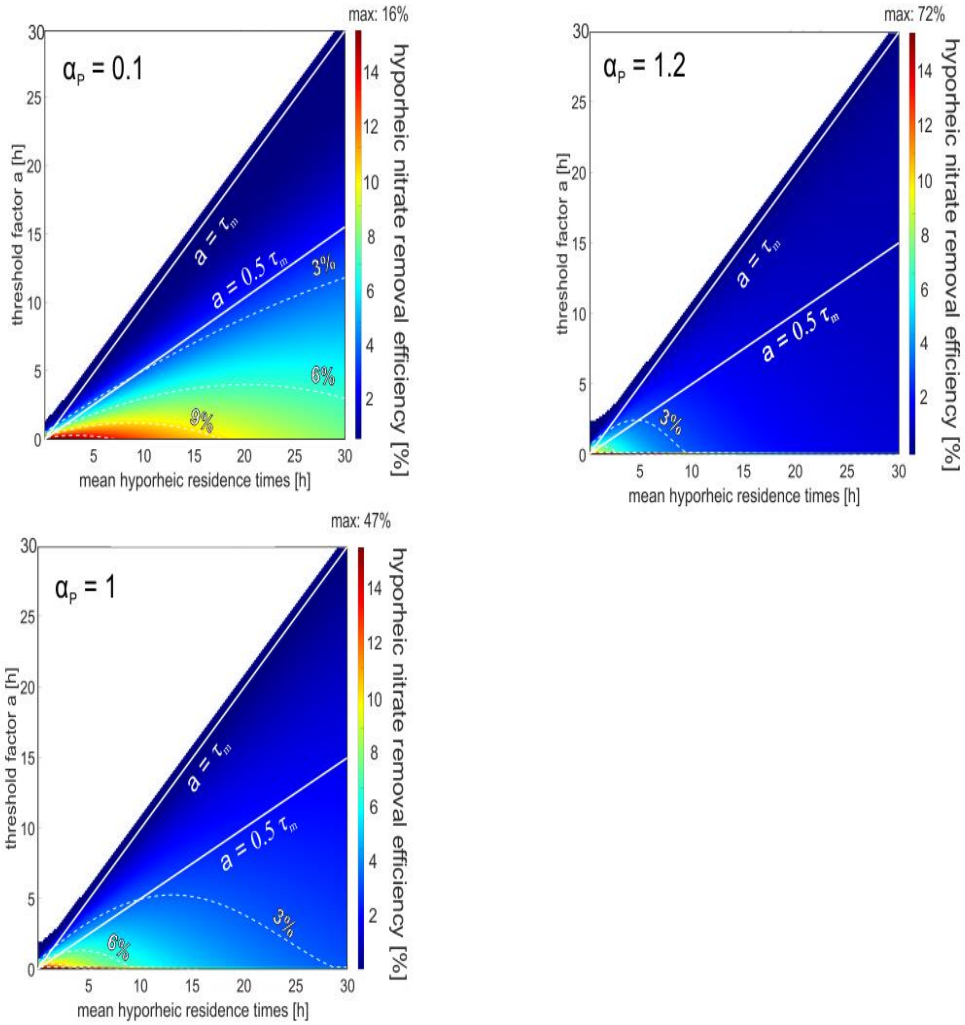

Figure 5: Simulated hyporheic nitrate removal efficiencies for the generic river reach using different parameter sets for mean resident times τ_m, threshold factors a and shape factors α_P for power law RT distribution models. The blanked areas above the 1:1 line result from an A_r factor lying close to zero resulting in a singularity when Equation 2 is calculated.

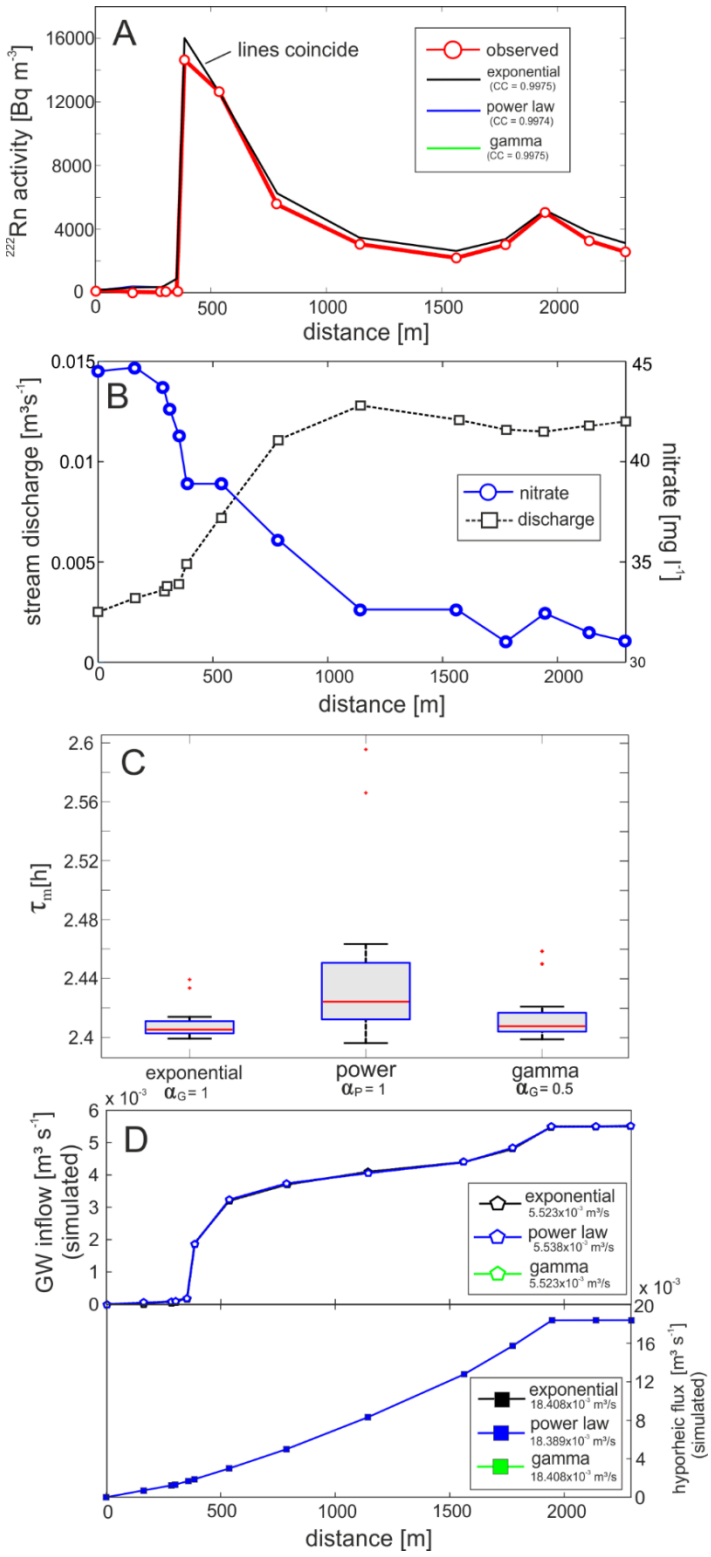

Figure 6: Simulated and observed in-stream ^{222}Rn activity (A); measured discharge and in-stream nitrate concentrations (B); Box-Whisker-Plots for the simulated mean hyporheic RT shown for the exponential (α_G = 1), gamma-type (α_G = 0.5) and power law (α_P = 1) distribution (C); modeled cumulative groundwater inflow and cumulated steady-state hyporheic water flux (D).

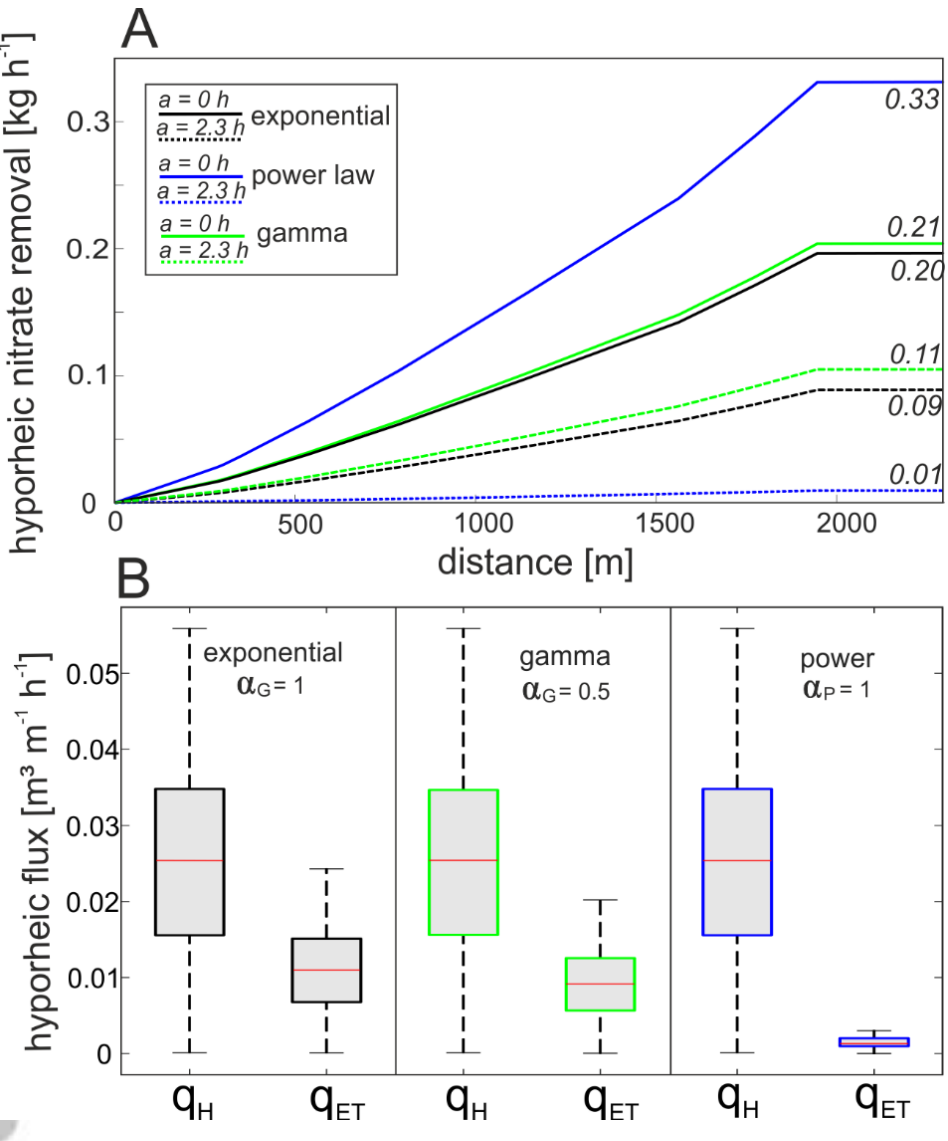

Figure 7: (A) Simulated hyporheic nitrate removal in the HZ by assuming $pdf_{RT} = pdf_{ET}$ (solid lines) and $pdf_{RT} \neq pdf_{ET}$ (dashed lines) shown for three different RT distribution models. Total values for all simulated RT distribution scenarios are shown in Table4. (B) Box-Whisker plots showing the variability of reach specific hyporheic exchange fluxes q_H and the effective hyporheic flux q_{ET} after introducing a threshold factor of a = 2.3 hours for the three different RT distribution models.

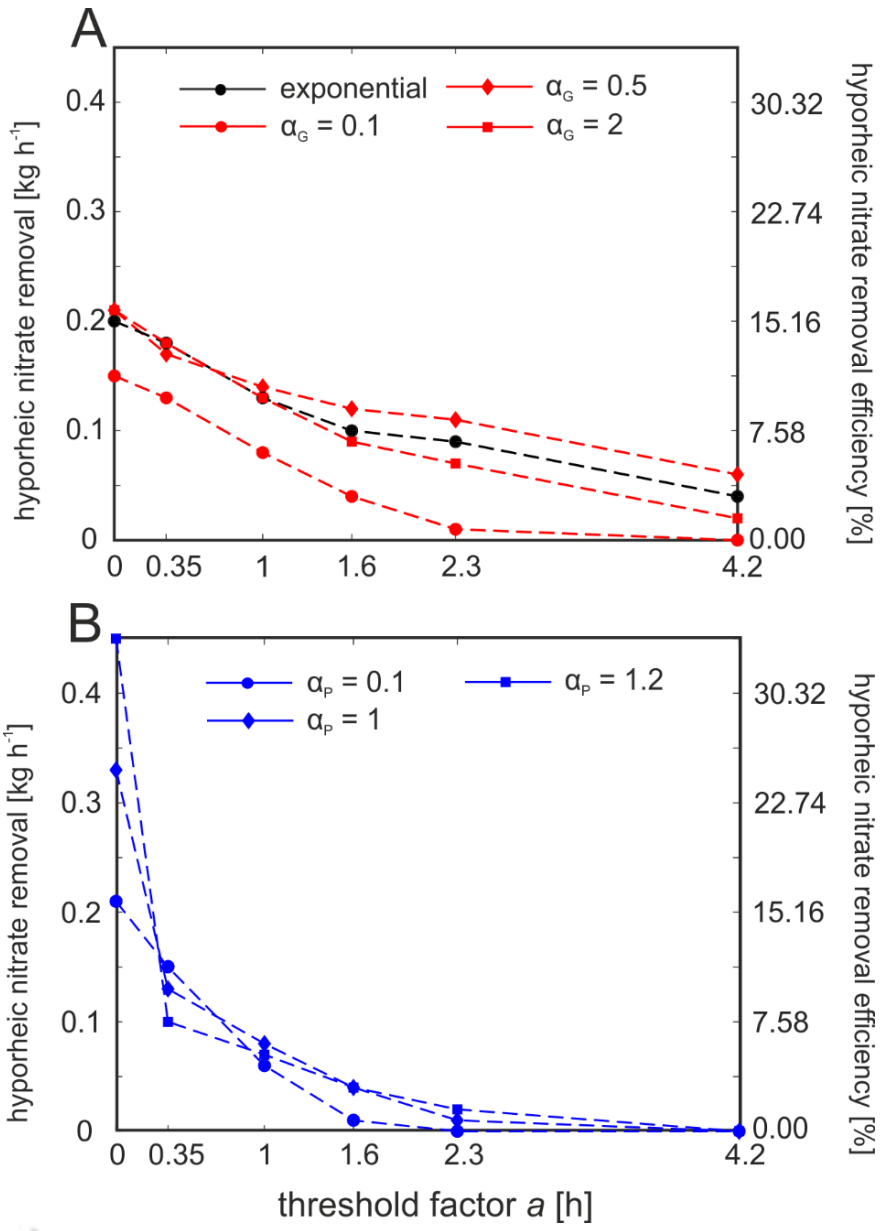

Figure 8: Cumulated hyporheic nitrate removal for all RT distribution scenarios for the 2.3 km stream reach for gamma-type/exponential pdf_{RT} (A) and power law pdf_{RT} (B).

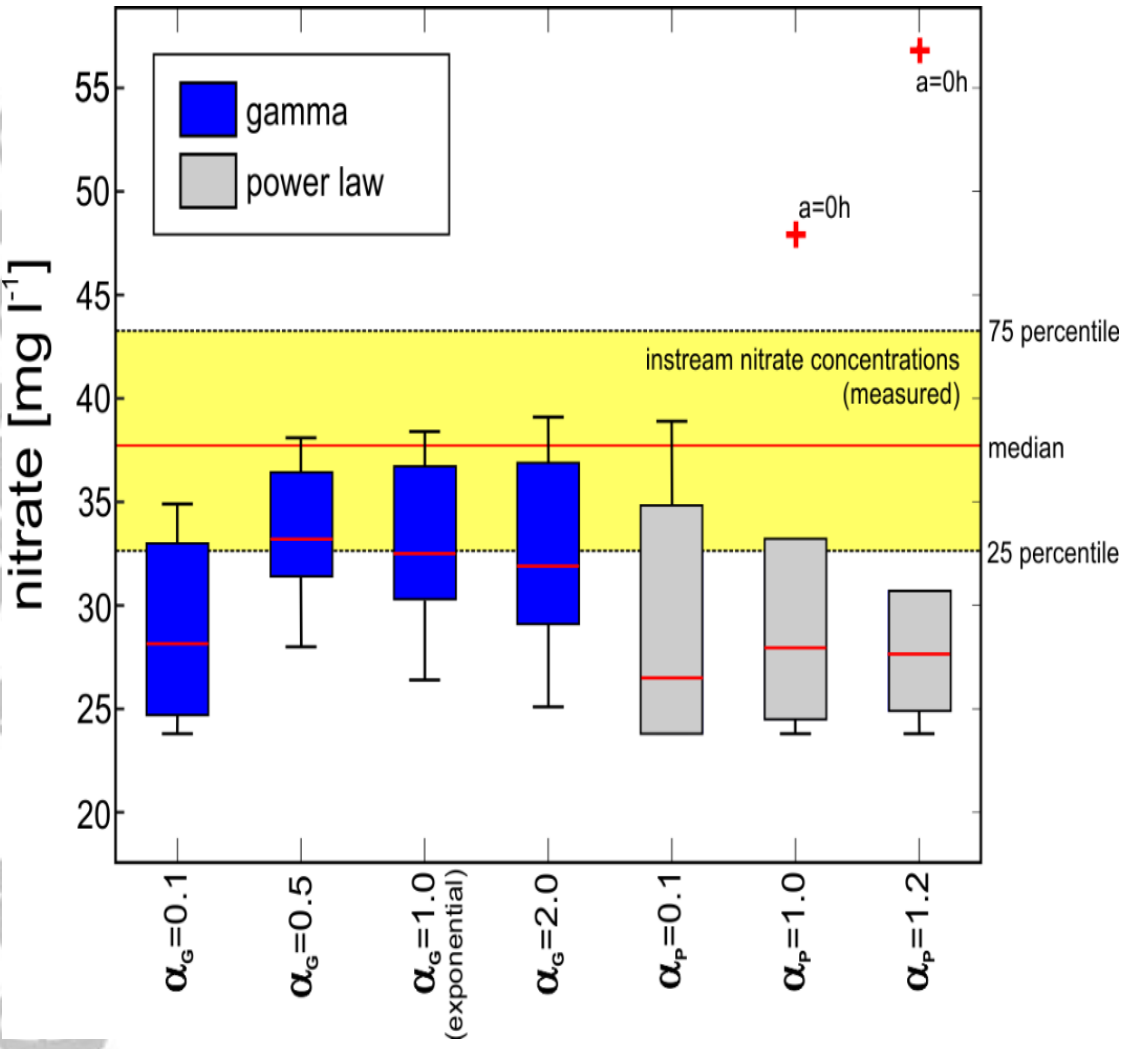

Figure 9: Observed in-stream nitrate concentrations and the nitrate concentration in the missing water source (e.g. farm drains) estimated for the different RT distribution scenarios.